Journal of Energy Storage 15 (2018) 103–123

Contents lists available at ScienceDirect

Journal of Energy Storage

journal homepage: www.elsevier.com/locate/est

Multi-axis vibration durability testing of lithium ion 18650 NCA cylindrical cells

James Michael Hooper[a,*], James Marco[a], Gael Henri Chouchelamane[b], Julie Sylvie Chevalier[b], Darren Williams[c]

[a] WMG, University of Warwick, Coventry, CV4 7AL, UK
[b] Jaguar Land Rover, Banbury Road, Warwick, CV35 0XJ, UK
[c] Millbrook Proving Ground Ltd, Millbrook, Bedfordshire, MK45 2JQ, UK

ARTICLE INFO

Article history:
Received 5 June 2017
Received in revised form 7 November 2017
Accepted 8 November 2017
Available online xxx

Keywords:
Six degrees of freedom (6DOF)
Multi-axis shaker table (MAST)
Electric vehicle (EV)
Li-ion battery ageing
Vibration
Durability

ABSTRACT

This paper presents new research to determine if the electromechanical attributes of Nickel Cobalt Aluminium Oxide (NCA) 18650 battery cells are adversely affected by exposure to vibration commensurate with that experienced by electric vehicles (EVs) through road induced excitation. This investigation applied vibration to a set of commercially available cells in six degrees of freedom (6-DOF) using a multi-axis shaker table. This method of mechanical testing is known to be more representative of the vibration experienced by automotive components, as 6 motions of vibration (X, Y, Z, roll, pitch and yaw) are applied simultaneously. Within the context of this study, cell characterisation within the electrical domain is performed via quantification of the cell's impedance, the open-circuit potential and the cell's energy capacity. Conversely, the mechanical properties of the cell are inferred through measurement of the cell's natural frequency. Experimental results are presented that highlight that the electromechanical performances of the 18650 NCA cells do not, in the main, display statistically significant degradation when subject to vibration representative of a typical 10-year European vehicle life. However, a statistically significant increase in DC resistance of the cells was observed.

1. Introduction

To help reduce the risk of excessive warranty costs and to ensure in-market reliability, automotive manufacturers perform a variety of *life representative* durability tests on components and sub-systems at the physical prototype stage of the vehicle design and development life-cycle [1–5]. Vibration durability testing via the use of electromagnetic or hydraulic shakers is one such test programme that is strategically employed when evaluating the suitability of different concept designs. The test programme is conducted to determine the durability of key vehicle components when subject to vibration energy that is representative of the in-service, real-world, environment. The importance of such tests is widely accepted within industry, as poorly integrated components, assemblies or structures subject to vibration can result in a significantly reduced service life [2,4,6–8]. In the worst case, catastrophic structural failure, through mechanisms such as fatigue cracking or work hardening of materials, may also occur [4,8].

Many electric vehicle (EV) manufacturers are adopting cylindrical format cells within the construction of their battery electric vehicle (BEV) and hybrid electric vehicle (HEV) battery assemblies [9,10]. Cylindrical cells are often chosen for integration within the rechargeable energy storage systems (RESS) for a combination of commercial and technical reasons, that include: built in safety features such as a current interrupt device (CID), excellent economies of scale due to their high manufacturing volumes and a dimensionally stable steel outer case making them easier to package within an EV module assembly [9–12]. However, there is currently limited data and evidence within industry or the academic literature that defines the impact that vibration energy may have on the performance or service-life of EV battery systems [13]. Much of the published research into the mechanical testing of EV cells is underpinned by the need for manufacturers to comply with mandatory transport legislation, such as UN 38.3 [14] and vehicle crash homologation [15]. Subsequently there has been a

* Corresponding author.
E-mail addresses: j.m.hooper@warwick.ac.uk (J.M. Hooper), james.marco@warwick.ac.uk (J. Marco), gchouch3@jaguarlandrover.com (G.H. Chouchelamane), jchevali@jaguarlandrover.com (J.S. Chevalier), darren.williams@millbrook.co.uk (D. Williams).

https://doi.org/10.1016/j.est.2017.11.006
2352-152X/

Nomenclature

6DOF	Six degrees of freedom
Ah	Ampere hour
ANOVA	Analysis of variance
ASD	Acceleration spectral density
BEV	Battery electric vehicle
CAE	Computer aided engineering
CC	Constant current
CID	Current interruption device
CT	Computer tomography
CV	Constant voltage
DC	Direct current
E	Young's modulus
EIS	Electrochemical impedance spectroscopy
EMS	Electromagnetic shaker
EOT	End of test
EV	Electric vehicle
g	Grams
g_n	The force of acceleration equivalent to gravity where $1g_n = 9.81$ m/s
HEV	Hybrid electric vehicle
I_{max}	Maximum applied current pulse
Li-ion	Lithium ion
MAST	Multi axis shaker table
mm	Millimetre
MPG	Millbrook proving ground
MSD	Millbrook structural durability
NCA	Nickle cobalt aluminium oxide
NMC	Nickel manganese cobalt
PLC	Programmable logic controlled
PPT	Power pulse test
RAC	Remote air conditioning
R_{CT}	Charge transfer resistance
R_{DC}	DC resistance of cells as measured by PPT
RESS	Rechargeable energy storage system
RMS	Route mean square
R_o	Ohmic resistance
S	Seconds
Smart ED	Smart electric drive
SOC	State of charge
SOT	Start of test
V_{10s}	Voltage after 10 s current pulse at imax
V_{OCV}	Voltage prior to the application of current pulse at imax
Wh/kg	Watt hour per kilogram
WMG	Warwick manufacturing group
X	X axis
Y	Y axis
Z	Z axis
ρ	Material density

clear focus on studies investigating mechanical robustness and crashworthiness via mechanical crush [16–18], penetration [19,20] and mechanical shock [16,21]. As discussed within [13], a limited body of research exists, for example presented in [21–26], which investigates the effect of vibration on li-ion cell chemistries via single-axis test methods. However, as highlighted within [13], the academic literature presents conflicting evidence with regard to the susceptibility of li-ion cells to vibration energy applied along a single-axis. A number of potential limitations exists that further compound the challenge of understanding the causality between vibration loading and the cell performance and ageing. Firstly, the single-axis vibration profiles employed within [21–26] are not representative of real-world EV use. The swept-sine waves utilised within the durability assessment of the cells [21–24] are equally deemed to be an unrealistic representation of the vibration loading that occurs within road vehicles [27]. Finally, the vibration profiles employed do not represent a known service-life condition, e.g. 100,000 miles of vehicle use, resulting in the data generated being unsuitable for the life estimation of the cells [13].

This study is an extension of previous published research to define the impact of vibration that is representative of 100,000 miles of vehicle durability on 18650 Nickel Manganese Cobalt (NMC) battery cells and 18650 Nickle Cobalt Aluminium Oxide (NCA) battery cells [13,28]. Within these studies, degradation in cell electrical and mechanical performance was observed, regardless of the cells' state of charge (SOC) or physical orientation. However, unlike complementary EV cell vibration studies, which have focused on conducting robustness and durability evaluation using single-axis vibration test methods [13,21–26,28], this research investigates the effect of vibration when applied in 6-degrees of freedom (6DOF) simultaneously. This was performed by subjecting cells to vibration signals measured from the battery assembly of a commercially available Smart ED vehicle when driven over industry standard proving ground durability surfaces. Unlike within [13,28] which apply vibration uni-axially within the frequency domain via the use of acceleration spectral density (ASD) profiles, this study applies the measured vibration within the time domain. The advantage of this methodology is that errors resulting from test time compression are avoided [2]. Also, because the vibration motion is applied in the time domain, it is more representative of real-world *in-vehicle* loading. As discussed within [29–32] within the context of traditional vehicle testing and component evaluation, the application of combined axial motions will often highlight additional failure modes that would otherwise not be observed through single-axis testing.

The primary objective of this research is to quantify the underpinning causality between the application of vibration energy and the cell's electrical performance and its mechanical attributes. This study also aims to identify if the *in-pack* orientation of the cells can influence the degree of mechanical and electrical ageing that may be observed. Within the context of this study, cell performance is quantified through the measurement of natural frequency, pulse power capability, electrochemical impedance spectroscopy (EIS) and discharge energy capacity. Full characterisation of the cells has been undertaken before and after vibration durability testing. An additional motivation for this study is to provide a comprehensive framework for multi-axis vibration testing within the field of EV battery test and evaluation that encompasses both the experimental set-up and an appreciation of key safety requirements and constraints. This paper is structured as follows: Section 2 provides a detailed description of the test methodology employed and the design of key test fixtures that are pre-requisite to the research. Section 3 presents the experimental results and quantification of the cell electrical performance and mechanical attributes before and after vibration durability testing. Statistical analysis is undertaken to identify if any change in cell performance is statistically significant. Discussion, Further Work and Conclusions are presented in Sections 4, 5 and 6, respectively.

2. Experimental method – multi-axis vibration durability testing in 6DOF

The test method employed within this study is summarised in Fig. 1. This section defines, in greater detail, the test methodology employed to better understand the durability and ageing behaviour 18650 NCA cells when subject to vibration energy in 6DOF that is comensurate with 10-years of EV service life.

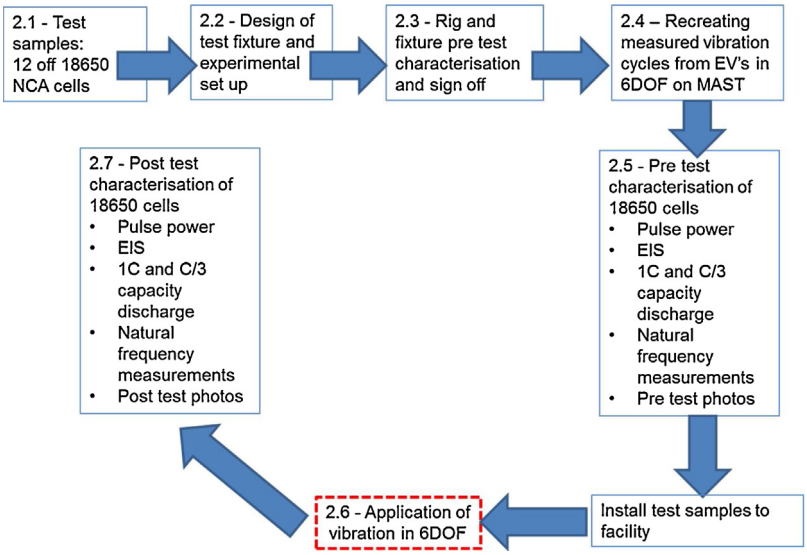

Fig. 1. Schematic of Test Process for Cells.

2.1. Test samples

Twelve 18650 3.1 Ah NCA cells were evaluated. The cells have a nominal voltage of 3.7 V. During this investigation, the 18650 NCA cells were assessed at an energy level of 75% SOC. 75% SOC was identified within a previous vibration durability study [13] as a charge state where increased cell degradation may be observed. The cells were divided into two batches. One batch comprised of 9 cells and was subject to the vibration profile in 6DOF. The remaining 3 cells were defined as control samples. The control samples were placed into storage at 10 °C for the duration of the test programme. Control samples that were not subject to vibration, were included to facilitate a more complete understanding of vibration related degradation relative to other ageing mechanisms, for example calendar ageing [33,34].

Cells are often packaged within different physical orientations, either within a single RESS or by different EV manufacturers exploring different design options. An example of this variation in cell packaging is the Tesla Model S that packages the 18650 cells in the Z orientation, whilst the Tesla Roadster packages the 18650 cells in the Y orientation. As a result, this study evaluates the effect of the three different X, Y and Z axis cell orientations, defined in Fig. 2. Details of each cell sample, including its orientation and unique identifier are defined in Table 1.

2.2. Experimental fixtures and commissioning

In order to provide a comprehensive understanding of the experimental method employed, a detailed description of the different cell mounting fixtures is provided. Particular consideration is given to those aspects of the methodology that are key for ensuring the safety of the test and for maintaining a high degree of test accuracy and repeatability.

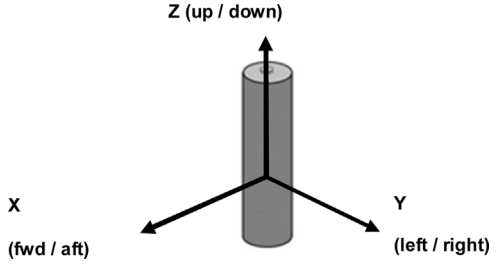

Fig. 2. The Three Cell Orientations Evaluated within this Study.

2.2.1. Cell fixtures

Fig. 3a presents one of three cell-mounting fixtures that were designed and fabricated to support vibration testing. Each fixture holds up to three cells and is intended to recreate a representative 18650 EV RESS mounting condition [13]. Three cell-mounting fixtures were manufactured to allow for the concurrent evaluation of multiple cells in different orientations during a single vibration test on the MAST [13]. The different cell orientations (X, Y and Z) were achieved by mounting the three cell fixtures onto the different surfaces of the cube shaped durability fixture illustrated in Fig. 3b [13]. To undertake resonance evaluations to mechanically characterise the cells at the start of test (SOT) and end of test (EOT), as discussed within Section 2.5.5, an additional cell resonance search plate was fabricated. This fixture is shown in Fig. 3c and was required to provide an interface with the single axis electromagnetic shaker table. The single-axis shaker was employed in the natural frequency measurement of the cells due to its frequency capability than the hydraulic MAST.

A detailed discussion into the design and manufacture of the different cell mounting fixtures is provided in [13] and will therefore not be repeated here. All vibration durability and assessment fixtures employed were constructed from 6082-T6 grade aluminium. This is due to the high Poisson's ratio associated with this material (circa: 0.33). Calculation of the Poisson's ratio is defined in Eq. (1), where the materials Young's modulus is defined as E and the density as ρ [35]. A high materials ratio (e.g. greater than 0.3) indicates a greater potential for a high natural frequency [35]. This is important to ensure that the fixture resonance is beyond that frequency range of the test. It must be noted however that the resonance behaviour of the fixture is

$$Poisson's\ Ratio = \frac{E}{\rho} \tag{1}$$

2.2.2. Test facility and setup

The complete test facility is shown in Fig. 4. The test rig employs a TEAM cube MAST. The MAST was installed within a climatic

Table 1
Test Sample Information.

Sample No	Test Profile	Orientation for Test
1	Data from Smart ED sequenced to 10-years European customer structural durability	Z
2		Z
3		Z
4		Y
5		Y
6		Y
7		X
8		X
9		X
10	Storage at a temperature of 10 °C	Control
11		Control
12		Control

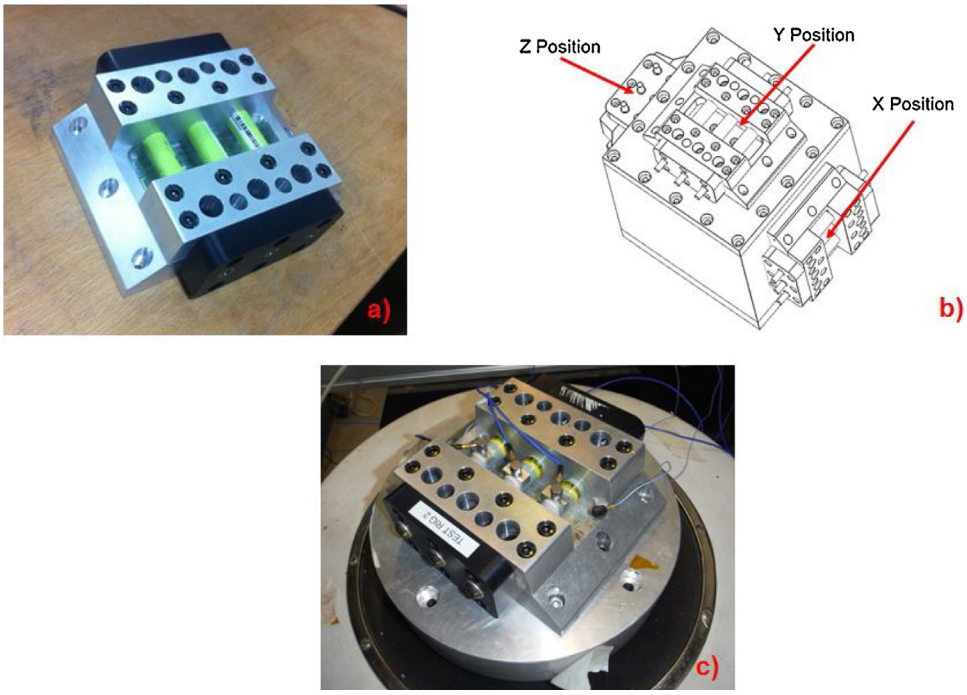

Fig. 3. a) Single Three 18650 Cell Holding Fixture, b) 18650 Block Fixture, c) Single Three 18650 Cell Holding Fixture on Resonance Search Plate.

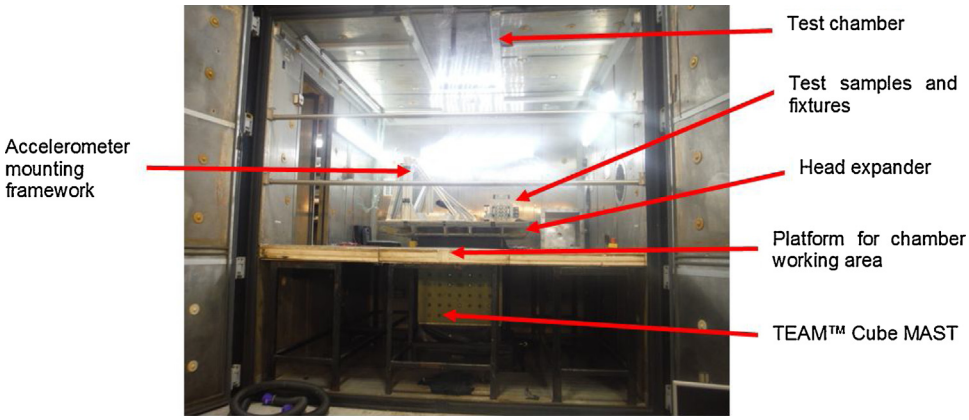

Fig. 4. MAST Vibration Test Facility at Millbrook Proving Ground.

chamber which, in turn, was connected to an L.Kel remote air conditioning (RAC) unit.

During testing, the ambient temperature was conditioned to 21 °C ± 3 °C. Within the test environment, K-type thermocouples and vibration sensors (accelerometers) were employed to provide test control accuracy and safety. To facilitate closed-loop vibration control, six blocks of three DJB Instruments A/130/V accelerometers were installed at key locations on the shaker table (discussed further in Section 2.4). A Labview PXie-1075 chassis with an integrated Ni-PXIe-8133 controller and input modules for 32 thermocouples (NI PXIe-4353), 4 channels for accelerometer measurements (NI PXI-4462) and a multifunctional data module (Ni PXIe-6363) were used for additional data recording and safety monitoring. The MAST was controlled by a Moog CC02310-301 test controller (Serial No 0069).

Several safety measures were included within the design of the test set-up. To safeguard against catastrophic cell failure, the test fixture was installed within a stainless-steel fire proof enclosure. The enclosure was fabricated from 3 mm thick 304 grade stainless steel. A gas Nitrogen injection system was integrated within the enclosure so that the test items could be placed into an inert environment if a significant increase in temperature was detected. Integrated with the enclosure was a programmable logic controlled (PLC) monitoring system that would automatically activate an audible alarm if the surface temperature of the cells is greater than 60 °C or a rate of increase greater than 4 °C/s is observed. The thermocouples were set to record at a rate of 1 sample a second.

A remotely activated gas extraction system was installed into the climatic chamber and the test enclosure to allow for the forced extraction of potentially harmful gases. Gas monitoring was performed remotely through air sampling via a RKI Instruments Eagle gas analyser Serial No (04-021-118) at a measurement sample interval of 30 s. This system would also output an audible alarm if hazardous quantities of hydrofluoric gas (>1 part per million), unsafe oxygen levels (<19%) or any hydrocarbons were detected.

The base plate of the fixture was fabricated from 25 mm thick 6082-T6 aluminium and contained cast nylon inserts. Cast nylon was incorporated into the fixture design to reduce the risk of an electrical earth path being created from the test item to the MAST. 10 mm thick G10 (fibre glass epoxy laminate) sheeting was placed between the test fixture and MAST to reduce heat transfer to the cast magnesium alloy components of the MAST. The G10 sheeting also provided additional electrical insulation between the NCA cells and the facility. Fig. 5 illustrates the test set up on the MAST.

2.3. Rig and fixture pre-testing characterisation and commissioning

The primary requirement of durability testing is to ensure that the vibration profile demanded by the electronic controller is faithfully applied to the samples under test. This is generally achieved by designing the experimental fixture to maximise the transmissibility of the vibration energy from the shaker table to the sample whilst concurrently minimising any unrepresentative cross-axis behaviour [13,28]. It is widely acknowledged as best practice to evaluate the vibration response characteristics of fixtures prior to commencing durability testing [35–37]. This is to ensure that no resonances which could affect the accuracy and control of the test occur within the shaker assembly itself. The term *Transmissibility* is a comparison of the output signal to the input signal [36] and is determined by the pre-test experimental evaluation of the fixture. Fixtures are characterised via a swept sine resonance search prior to testing to ensure that no significant resonances occur in the three axes of the vibration fixture. Prior to evaluating the fixtures and prior to commencing any vibration study [38–40], it is also necessary to fully understand the frequency response of the MAST. This is to ensure that the MAST does not exhibit a resonance within the frequency range of the durability test. Within the context of this study, this was 1–110 Hz. A further requirement is to ensure that the MAST does not generate any vibration spectra which could create unrepresentative failure modes to occur.

This section presents the results from the pre-test evaluation of the MAST and the transmissibility of the cell mounting fixtures. This evaluation was conducted as follows:

- Assessment of the MAST for resonances in the X, Y and Z axis at 1 g_n (g_n is the force of acceleration equivalent to gravity where 1 g_n = 9.81 m/s) over a frequency range of 1–110 Hz at 1 octave/min.
- Modal analysis of fixtures
- Assessment of 18650 fixtures and resonance search plate when evaluated in accordance with BS EN 60068

2.3.1. Frequency response of multi-axis shaker table (MAST)

The vibration frequency response of the MAST was measured using a swept sine wave of amplitude 1 g_n over a frequency range of 1–110 Hz at 1 octave/min. Four accelerometers were placed in the X, Y and Z axis across the head expander of the TEAM cube MAST on bespoke aluminium mounting blocks. The table was excited in the Z axis and the cross axis motion was measured. Upon analysing the

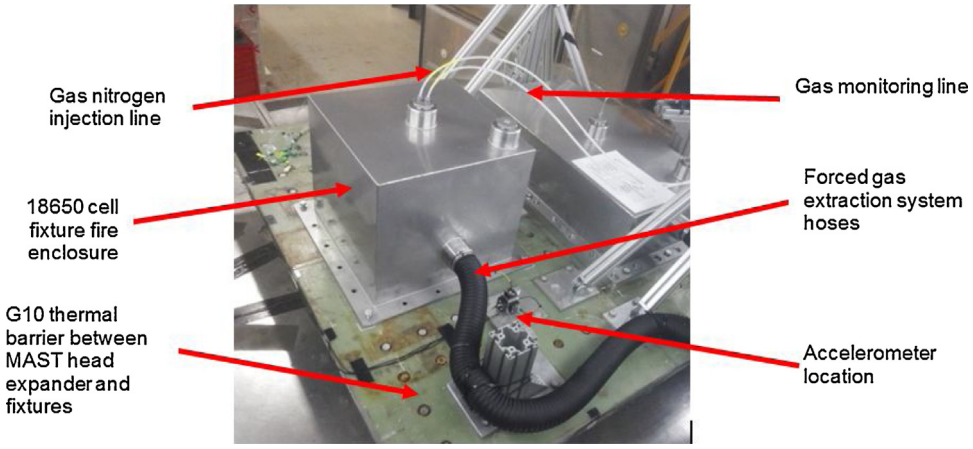

Fig. 5. Multi Axis Shaker Rig Assembly.

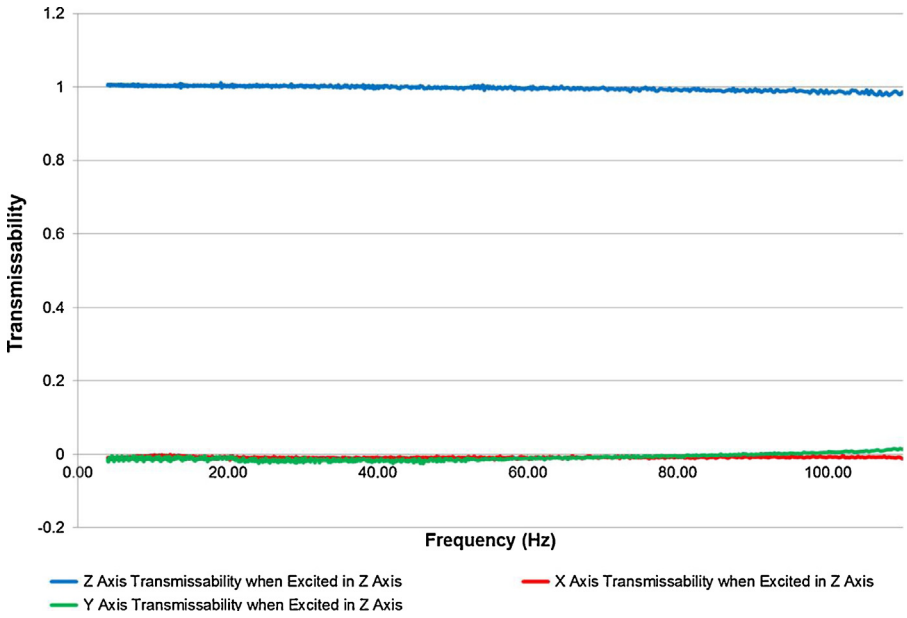

Fig. 6. Transmissibility of MAST when Excited in Z Axis.

response of the MAST, no significant resonances or cross axis motion was identified that would detrimentally impact the accuracy or reliability of the durability test programme. The transmissibility of MAST is presented in Fig. 6.

2.3.2. Vibration response of 18650 fixtures and resonance search plate when assessed via impact excitation modal analysis

Prior to placing the fixtures on their respective shaker facilities, their modal performance was assessed using impact excitation, via hammer surveying techniques using a single input multiple output (SIMO) method. This was undertaken to determine their suitability for conducting the durability testing, through the identification of their mode shapes and the first modal frequencies. The test method utilised within this study is discussed in detail within this section, however the supporting theory behind modal analysis is presented in [41–44].

With this method several measurement accelerometers are attached to the test item at multiple locations. The input excitation is applied to the test item at a single location via a calibrated aluminium tipped impact hammer (with built-in load cell). Each point is assessed individually before being combined to determine the modal behaviour of the test fixture. The assembled durability fixture and the resonance search plate (with a single cell fixture installed) were both marked with a suitable grid density to ensure that enough measurements were recorded to accurately determine their mode shapes. A picture of the three dimensional grid pattern and corresponding photographs are presented in Figs. 7 and 8, for the durability fixture and resonance search plate assembly respectively. The dimensions for the grid patterns (and subsequently the basic dimensions of the fixtures) are presented in Tables 2 and 3. The axis conventions for the modal analysis testing is also illustrated in Figs. 7 a and 8 a.

The testing was conducted using a 140 g “Brüel and Kjær”8206 impact hammer with head extender. This was used in conjunction with five multi axis “Brüel and Kjær TEDS 4535-B-001” accelerometers. The data logger analyser used within this experiment was a “Brüel and Kjær 3053-B-120 Input Output Controller” which was combined with a “Brüel and Kjær 3660 type C chassis”. The 0.14 kg hammer with an aluminium tip provided a measurement frequency range of approximately 0–5000 Hz. The reason why this

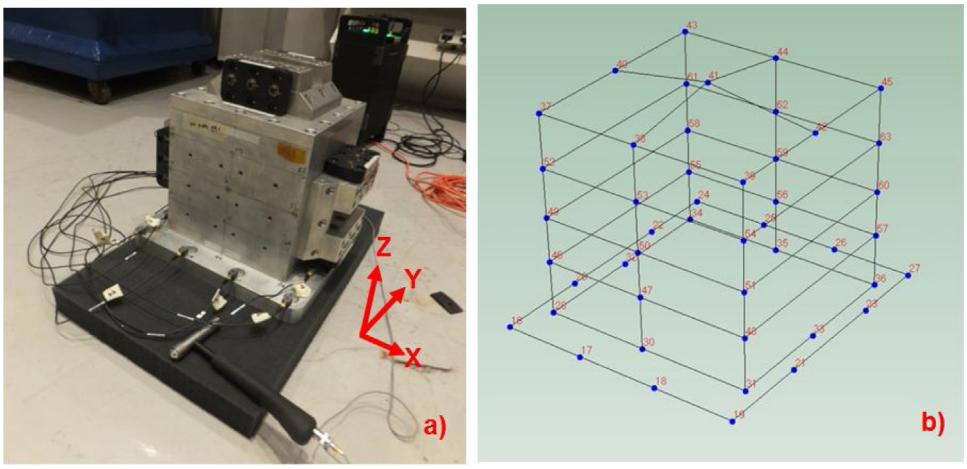

Fig. 7. a) Test Set Up and Axis Convention of Durability Fixture for Modal Analysis, b) Node Positions and Numbers of Durability Fixture.

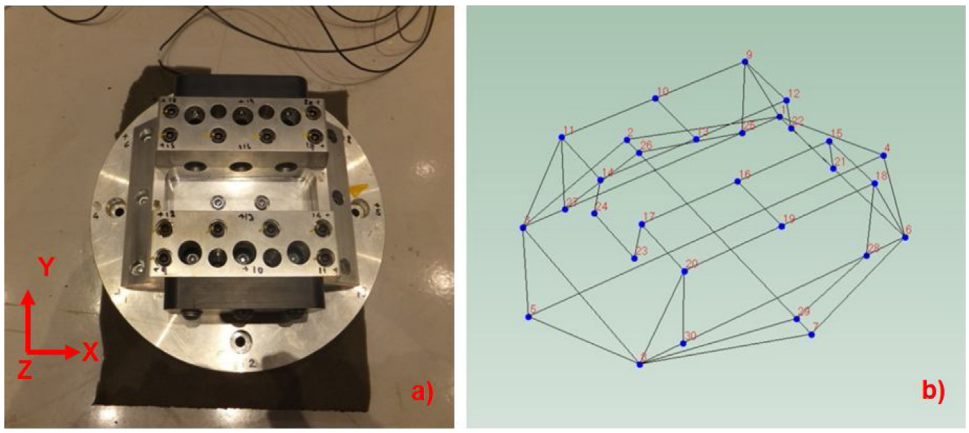

Fig. 8. a) Test Set Up and Axis Convention of Resonance Search Plate for Modal Analysis, b) Node Positions and Numbers of Resonance Search Plate.

Table 2
X:Y:Z Node Coordinates/Measurements for Durability Fixture.

	X:Y:Z Coordinates in mm		
Node Number	X	Y	Z
16	0	0	0
17	0	100	0
18	0	200	0
19	0	300	0
20	110	0	0
21	110	300	0
22	250	0	0
23	250	300	0
24	340	0	0
25	340	100	0
26	340	200	0
27	340	300	0
28	50	20	0
30	50	145	0
31	50	280	0
32	175	20	0
33	175	280	0
34	300	20	0
35	300	145	0
36	300	280	0
37	50	20	245
38	50	145	245
39	50	280	245
40	175	20	245
41	175	145	265
42	175	280	245
43	300	20	245
44	300	145	245
45	300	280	245
46	50	20	65
47	50	145	65
48	50	280	65
49	50	20	120
50	50	145	120
51	50	280	120
52	50	20	180
53	50	145	180
54	50	280	180
55	300	20	65
56	300	145	65
57	300	280	65
58	300	20	120
59	300	145	120
60	300	280	120
61	300	20	180
62	300	145	180
63	300	280	180

frequency band was chosen was so that the primary modes could be determined within the test frequency ranges of 1 to 110 Hz (for the durability fixture) and 5 to 3700 Hz (for the resonance search plate assembly). The data was sampled at 3.2 times the desired peak frequency in accordance with Shannon's sampling theorem. The weight of the accelerometers mounted to the DUT was no greater than 0.001% of the total weight of the lightest fixture, thus minimising the result of experimental error by the introduction of additional weight. The accelerometers were fixed via the use of "petro wax" so that no surface or structural change was introduced by the application of permanent adhesives.

Each fixture was placed on suitable polyurethane foam pads and the response at each node location (defined within Figs. 7 and 8) was measured when the fixture was excited with five impacts at a single point. The five impacts were averaged to generate a single input and single output response for the given test location for the excited axis. The durability fixture was excited in X, Y and Z axis by applying an X axis excitation at node 45, a Y axis excitation at node 39 and a Z axis excitation at node 37. The resonance search plate was excited in the Z axis only at node 100 as this fixture assembly was subjected to multi-axial vibration during this study. Within the modal assessment, the durability fixture was evaluated without cells, whilst the resonance search plate was evaluated both with and without 18650 cells installed. The durability fixture was evaluated without cells as the preliminary results of the fixture displayed a significantly high degree of separation between the test frequency range and the first natural frequency. It was deemed that the additional mass loading provided by the inclusion of cells to the fixture (<1%) would not impact the suitability of the fixture for durability testing.

Within this investigation the data was post processed using the "PULSE Reflex Version 21" software within the Brüel and Kjær modal analyser to generate the desired information for the fixtures. A single FRF from each test position was evaluated together using its global curve fitting application to generate a single FRF trace which represented the modal performance of the whole module. The modal properties of natural frequency were extracted by the PULSE Reflex software. Mode shapes were also estimated from the FRF's using the PULSE Reflex software.

The first three modes and mode shapes for the durability fixture are presented in Table 4 and Fig. 9. As discussed in greater detail in Section 2.4, during the multi-axis durability test, the fixture will been excited to a peak frequency of 110 Hz. The first mode of the durability fixture occurs between 2070 and 2074 Hz, which is approximately 20 times greater than the peak test frequency of the durability test. This indicates that the chance of modal excitation within the test fixture during the durability test will be low and

Table 3
X:Y:Z Node Coordinates/Measurements for Resonance Search Plate.

	X:Y:Z Coordinates in mm		
Node Number	X	Y	Z
1	0	0	0
2	97.5	−35	0
3	195	0	0
4	−35	67.5	0
5	230	67.5	0
6	0	135	0
7	97.5	170	0
8	195	135	0
9	30	0	60
10	97.5	0	60
11	165	0	60
12	30	45	60
13	97.5	45	60
14	165	45	60
15	30	90	60
16	97.5	90	60
17	165	90	60
18	30	135	60
19	97.5	135	60
20	165	135	60
21	25	90	35
22	25	45	35
23	170	90	35
24	170	45	35
25	30	0	0
26	97.5	−20	0
27	165	0	0
28	30	135	0
29	97.5	155	0
30	165	135	0
100	30	42	0

that the fixture is suitable for testing. These results also indicate a good level of cross axis correlation between observed mode shapes and natural frequencies when excited in the X, Y and Z axis.

With respect to the results from the resonance search plate fixture presented in Table 5 and Fig. 10, the first mode of the fixture with cells installed is approximately 167 Hz greater than the peak frequency of the single axis EMS employed for the swept sine evaluation of the cells. The inclusion of the cells within this fixture increased the first natural frequency by approximately 30 Hz, and reduced the second natural frequency by approximately 6 Hz.

In summary both fixtures, when evaluated using impact excitation in the free–free condition, had first natural frequencies and corresponding mode shapes outside the frequency range of the desired test excitation. However because the response of the fixtures will change when clamped to the shaker tables, additional assessments were conducted once installed to their respective facilities to ensure their suitability for testing. These assessments are discussed in Section 2.3.3.

2.3.3. Vibration response of 18650 fixtures and resonance search plate when assessed in accordance with BS EN 60068

To ensure that the fixtures did not display any significant resonances once bolted to the test facility, all cell mounting fixtures were evaluated in accordance with BS EN 60068 prior to testing. This specification requires that *the maximum vibration amplitude in any axis perpendicular to the specified axis shall not exceed 50% of the specified amplitude up to* 500 Hz [40]. The 18650 fixture was excited in the Z-axis via a swept sine wave of amplitude 1 g_n over a frequency range from 1 to 110 Hz at a rate of 1 octave per minute on the TEAM Cube MAST. The measured vibration response in all three axes, were within the limits specified by BS EN 60068. The resonance search plate fixture was also evaluated in accordance with BS EN 60068 and was excited in the Z axis via a 1 g_n swept sine from 5 to 3700 Hz at a sweep rate of 1 octave/min on the single axis VP85 EMS. The resonance search plate with a single 18650 three cell fixture installed met the requirements of BS EN 60068 from 5 to 3700 Hz. The transmissibility plots for the durability fixture and resonance search plate are presented in Figs. 11 and 12 respectively. Additional information relating to the resonance search plate fixture evaluation is presented in [13]. It is hypothesised that a drop in transmissibility within Fig. 12 at approximately 1550 Hz is the result in the interaction between the

Table 4
First Three Modes Observed within Durability Fixture when Excited in X, Y and Z Axis.

	When Excited in Z Axis (Node 37)		When Excited in Y Axis (Node 39)		When Excited in X Axis (Node 45)	
Mode Number	Frequency (Hz)	Mode Shape	Frequency (Hz)	Mode Shape	Frequency (Hz)	Mode Shape
1	2070.56	Side panels panting	2071.70	Side panels panting	2074.91	Side panels panting
2	2525.29	Top panel panting	2522.67	Top panel panting	2521.55	Top panel panting
3	2623.53	Base Torsional	2618.37	Base Torsional	2623.80	Base Torsional

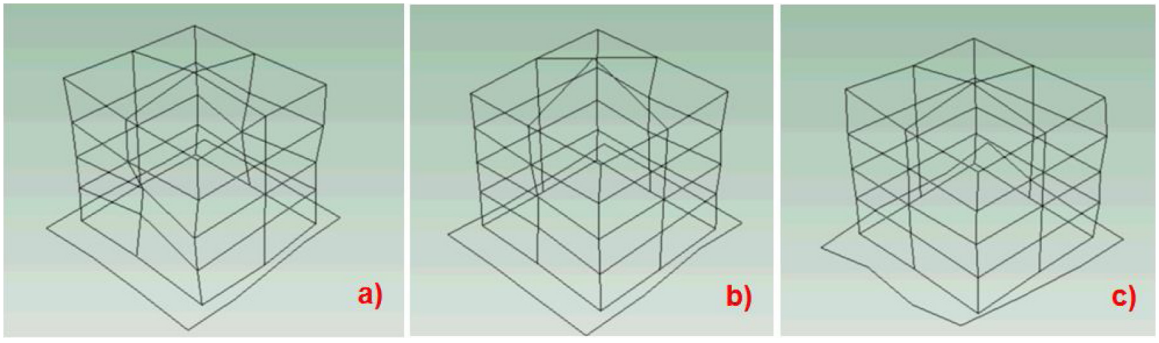

Fig. 9. Examples of Mode Shapes Observed in Durability Fixture (for Z axis Excitation) – a) 2070.56 Hz Side Panels Panting, b) 2525.29 Hz Top Panel Panting, c) 2623.53 Hz Base Torsional.

Table 5
First Two Modes Observed within Resonance Search Plate when Excited in Z axis, both with and without Cells Installed.

	When Excited in Z Axis without 18650Cells installed (Node 100)		When Excited in Z Axis with 18650Cells installed (Node 100)	
Mode Number	Frequency (Hz)	Mode Shape	Frequency (Hz)	Mode Shape
1	3837.93	Bending	3867.22	Bending
2	4128.12	Bending	4122.21	Bending

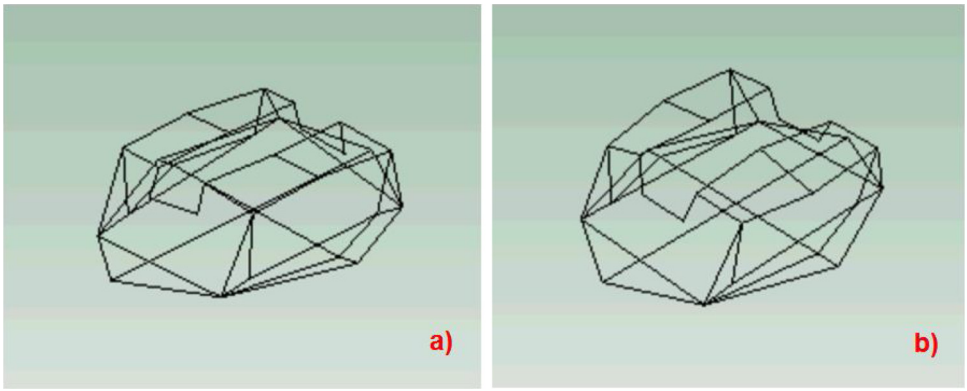

Fig. 10. Examples of Mode Shapes Observed in Resonance Search Plate (with Cells Installed) a) 3867.22 Hz Bending, b) 4122.21 Hz Bending.

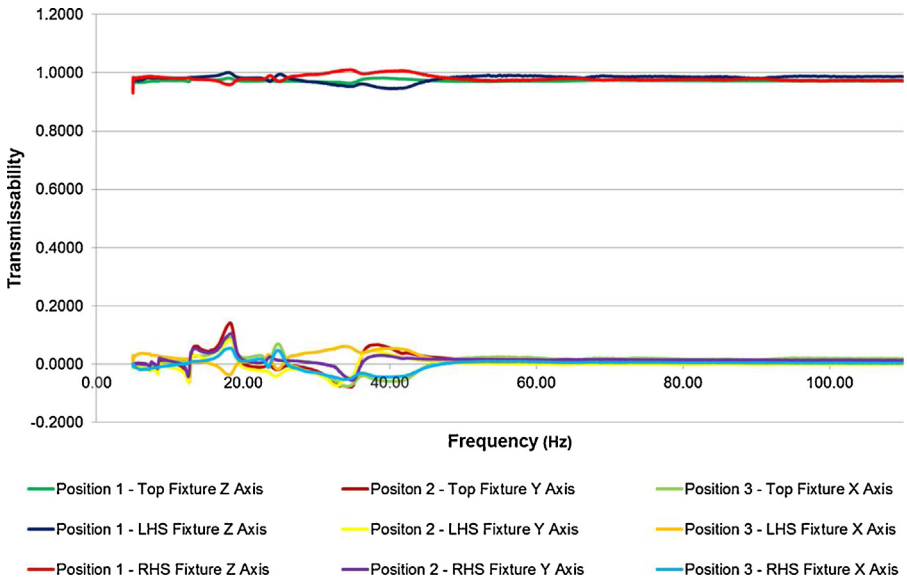

Fig. 11. Transmissibility Plot of Durability Fixture from 1 to 110 Hz when Excited in the Z axis.

resonance search plate fixture and shaker table armature. All transmissibility evaluations on the fixtures were conducted without test samples installed.

2.4. Recreating measured vibration cycles from EV's in 6DOF on MAST

With a 6DOF vibration test, measured vibration signals are applied in the time domain to the system under test. This study employed the vibration measurements from the Smart ED vehicle, which were recorded as part of the research presented within [2,45,46]. These measurements included the response of the battery assembly as the vehicle was subject to specific durability surfaces at the Millbrook Proving Ground (MPG) within the UK. The Smart ED was chosen for the 6DOF cell durability study, as its compact dimensions and suspension geometry results in high levels of vibration energy at frequencies below 5 Hz. Also the X and Y axis vibration loads are significantly higher than other current production EVs measured within [2,45,46]. Furthermore, the Smart ED has a battery assembly constructed of 18650 type cells, which therefore has a greater correlation to the test samples under assessment within this investigation.

The Millbrook Structural Durability (MSD) test framework [47] was employed to define the number of repeated road surfaces that would be sequenced together to replicate a vehicle durability life. This framework defines the durability surfaces and number of required repeats of each surface to replicate 10 years of typical European customer use. While this procedure represents an internal organisational standard, it has evolved over 20 years of

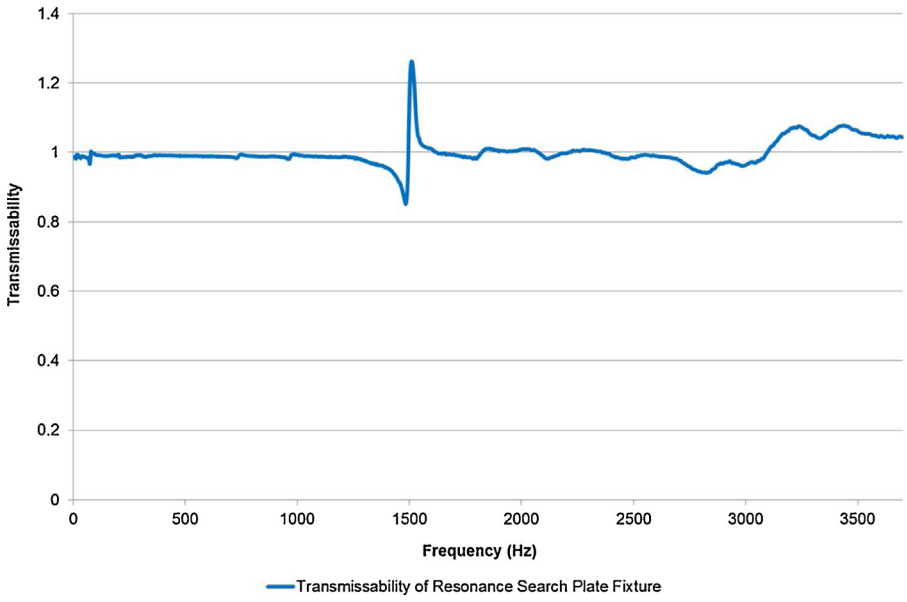

Fig. 12. Transmissibility Plot of Resonance Search Plate Fixture from 5 to 3700 Hz (Without Cells Installed).

Table 6
Surface Repeats for 10 Years European Millbrook Structural Durability [47].

Surface	Repeats of surface required for 10 Years European structural durability [47]	Revised number of repeats for 6DOF Study	Number of repeats of surface for 1 loop (total 300 loops required)[a]	Edited duration of surface (seconds)	Total duration of surface with surface repeats for one loop (seconds)
Hill route (loop 1)	3365	3600	12	22	264
City course	6570	6600	22	13	286
Twist humps	1800	1800	6	33	198
Sine waves	1204	1200	4	34	136
Random waves	1200	1200	4	85.5	342
Belgian pave	600	600	2	134	268
Cats eyes – 30 mph	600	600	2	29	58
Cats eyes – 50 mph	600	600	2	57	114
HSC	420	600	2	11	22
Handling circuit	219	600	2	110	110
Pot holes[b]	54	60	1[b]	32	32
Mile Straight – Wide open throttle	1200	0	0	0	0
Mile Straight – Part open throttle	1200	0	0	0	0
Total		–	–	–	**1830**

[a] This sequence is repeated 300 times to achieve 150.36 h test duration (approximately 10 years EV customer usage).
[b] perform once every 5 loops of surfaces.

experience and is currently employed by a number of leading vehicle manufacturers to assess the service life of their products [45].

Unlike standards employed in previous cell vibration durability studies, discussed in [13,21,28] and employed by other researchers, for example [24], the MSD standard defines life in years as opposed to vehicle mileage. However, approximately 15,000 miles of proving ground driving represents 10 years of typical customer structural degradation [47]. A summary of surface repeats required for the standard procedure is shown in Table 6.

Testing for this study was limited to 150 h. To ensure that the desired number of surfaces could be replicated within a 150 h test duration on the MAST; significant periods of "non-damaging" vibration (e.g. measured vibration that was less than 0.1 g_n) was deleted from each of the axis-signals. This is a common method with regard to reducing test time and hence test costs [7]. To maximise the available test time, additional surface repeats for the hill route, handling circuit and high speed circuit were added to the test schedule. The revised number of surfaces and associated number of repeats are defined in Table 6. To ensure a representative even loading of surfaces was achieved the signals were replicated in surface-loops. A surface-loop is defined as a block of multiple surfaces which lasts approximately 30 min and contains a weighted number of repeats for each surface defined in Table 6.

Each loop of signals was repeated 300 times to achieve the desired 150 h vibration test profile. The surfaces were applied in blocks of sequenced surfaces to ensure an even fatigue loading during the testing. It is desirable to apply a balanced and mixed surface loading so that a representative operational life is replicated, as it is unlikely that a vehicle will be exclusively subjected to one particular driving event for any prolonged period of time during customer use.

When replicating recorded data in the time domain on a MAST it is necessary to ensure that the six control multi-axis accelerometers are installed in the same X, Y and Z locations on the test rig to that of the measurement vehicle. Within this study, the upper, front right corner mounting hole on the cube head expander was taken as the 0:0:0 coordinate origin for the X:Y:Z measurements for the control accelerometers. The locations of the accelerometers from the measurement vehicle were then transposed to the MAST expander. A physical frame was constructed to ensure the accelerometers could be installed in the correct locations to emulate the in-vehicle measurement locations. The frame assembly and the accelerometer locations are presented in Fig. 13 and Table 7.

This frame was suitably ridged to ensure that no disrupting resonances within the frame itself occurred within the desired test frequency range of 1–110 Hz. During data-recording the vibration signals were filtered with a low pass filter with a cut-off frequency of 110 Hz. Signal noise was clipped to $3\,g_n$ in-line with the capabilities of the shaker system. An example of the typical frequency response of the cube against the original measured

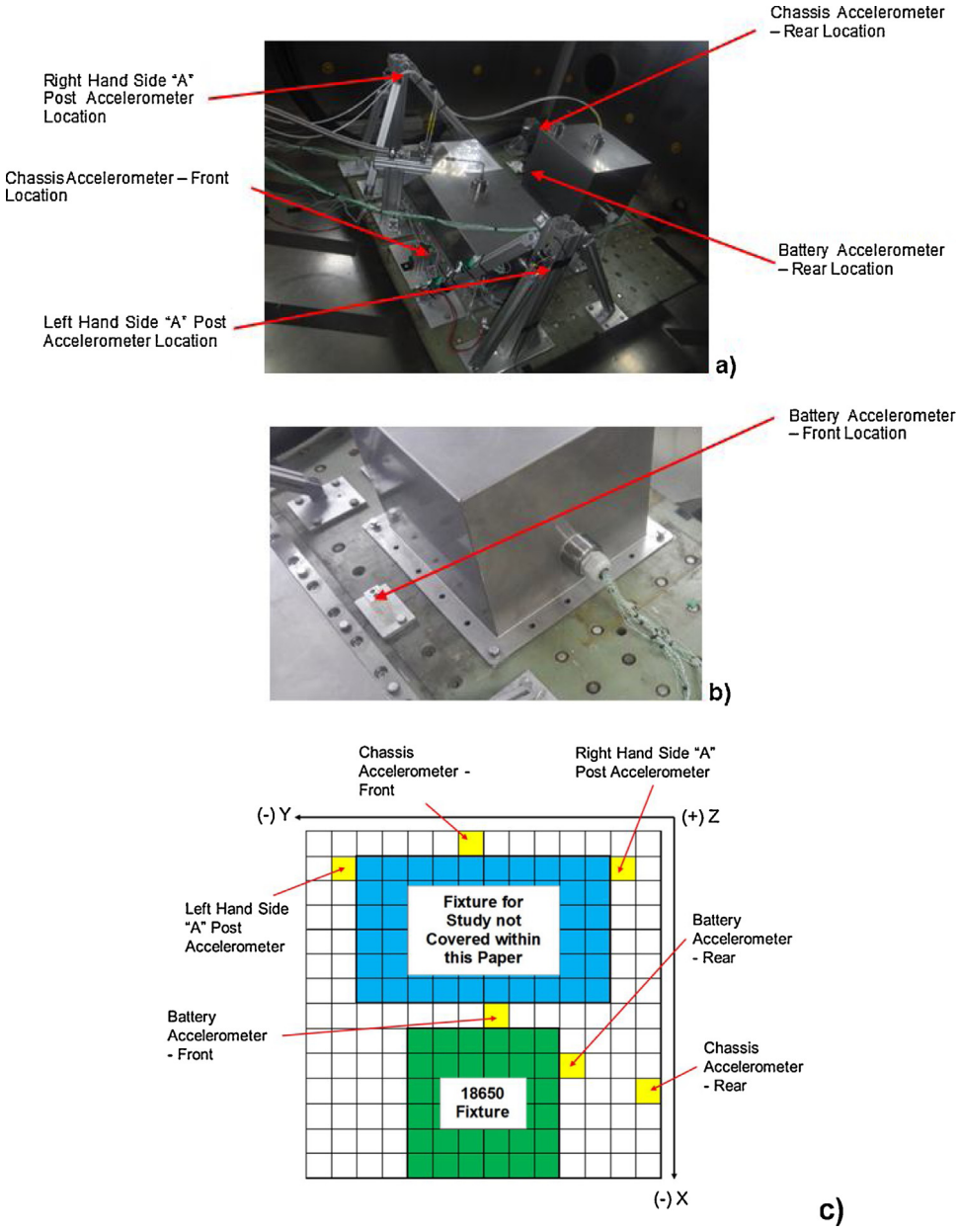

Fig. 13. a) Accelerometer Frame Assembly and Accelerometer Locations, b) Battery Accelerometer – Front Location, c) Schematic of Table and Accelerometer Locations Including Measurement Convention of Accelerometers.

Table 7
Accelerometer X:Y:Z Co-ordinates on Head Expander.

	X:Y:Z Coordinate Measurements on Shaker Table (in mm)		
Accelerometer Location on Vehicle	X	Y	Z
Right Hand Side "A" Post Accelerometer	0	0	530
Left Hand Side "A" Post Accelerometer	0	−1260	525
Battery Accelerometer – Front	−580	−550	0
Battery Accelerometer – Rear	−840	−190	0
Chassis Accelerometer – Front	100	−705	60
Rear Chassis Accelerometer – Rear	−980	10	160

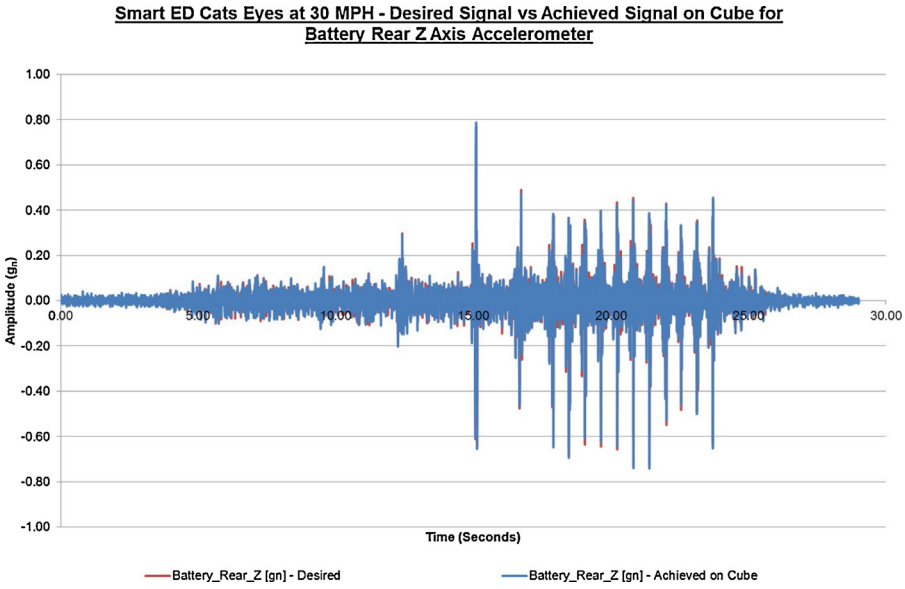

Fig. 14. Smart ED – Cats Eyes at 30 MPH – Desired Signal vs Achieved Signal – Z Axis.

signal is shown in Fig. 14. Please note that an ASD of the signals combined to replicate 100,000 miles of durability utilised within this study is presented in [2].

2.5. Electrochemical characterisation before the application of vibration

The following characterisation tests were performed on all cells defined in Table 1 at SOT. Measurements were recorded in a thermally controlled environment at a temperature of 21 °C ± 0.5 °C. The exception to this was the natural frequency measurements which were conducted in a laboratory environment at a temperature of 21 °C ± 3 °C.

2.5.1. SOC adjustment process

Cell SOC was adjusted by fully charging the cells with a constant current (CC) of amplitude 1.1 A–4.2 V followed by a constant voltage (CV) charging phase until the current fell to 0.05 A. At the end of charge, the cells were allowed to rest for 4 h prior to being discharged at 1 C for 15 min or 30 min to achieve a SOC of 75% or 50% respectively. The cells were then allowed to rest for a further 5 h to ensure that they had reached equilibrium.

2.5.2. 1C and C/3 capacity measurement

The cells were fully charged using the CC-CV process defined in Section 2.5.1. The cells were allowed to rest for 4 h prior to being discharged at 1C to the manufacturer's defined cut-off voltage of

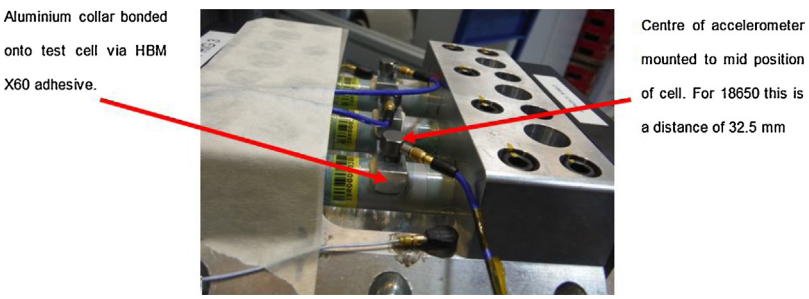

Fig. 15. Location of Cell Accelerometer for Natural Frequency Measurement via Swept Sine Frequency Sweep.

2.75 V. The energy extracted was recorded as a measure of the cell's 1C energy capacity. After a 4 h rest the process was repeated, but the discharge current was reduced to C/3 and to lower voltage limit of 2.75 V. The energy extracted was recorded as a measure of the cell's C/3 energy capacity.

2.5.3. Pulse power discharge resistance

To determine the DC resistance of the cells (R_{DC}), a series of current pulses were applied to the cells after they were conditioned to 50% SOC. Each current pulse is 10 s in duration with a magnitude of 20, 40, 60, 80 and 100% of the cell's rated maximum pulse discharge current of 4.4 A [28]. Between successive discharge pulses, the cells were allowed to rest for 30 min. The DC resistance of the cell was approximated using Eqs. (2) and (3) for each excitation pulse (n); where V_{OCV} defines the voltage prior to the application of the current pulse (I_{max}) and V_{10s} is the cell voltage at the end of the 10 s current pulse [28]. An average value of R_{DC} was computed as the mean value of resistance from each of the five pulses as per Eq. (3).

$$R_{DC} = \frac{(V_{OCV} - V_{10s})}{I_{\max}} \tag{2}$$

$$R_{DC} = \sum_{n=1}^{n=5} \frac{R_{DC}}{n} \tag{3}$$

2.5.4. EIS measurement

The EIS measurement was undertaken in galvanostatic mode using ModuLab® electrochemical system model 2100A fitted with a 2 A booster card and driven by Modulab® ECS software [28]. The EIS spectra were collected within the frequency range of 10 mHz to 10 kHz with 10 frequency measurement points per decade [28]. The applied route mean square (RMS) value of the excitation current was set to 200 mA.

2.5.5. Natural frequency measurement

A single point natural frequency measurement was undertaken as at the start and end of test as a method of comparison of the cells mechanical performance. The natural frequency of each cell was measured by fastening the respective cell to a VP85 electromagnetic shaker (EMS) table and applying a swept sine wave from 5 to 3700 Hz, of amplitude 1 g_n at a rate of 1 octave/min [13]. As shown in Fig. 15, the response of the cell in relation to this 1 g_n excitation, was recoded via a lightweight, single-axis accelerometer. The measurement accelerometers (model PCB 352C65) were secured to the centre of the cell via a threaded aluminium collar which was bonded to the cell surface. These were attached to the cell via the use of HBM X60 adhesive. A strip of Capstan tape was placed between the cell and the adhesive to enable removal of the adhesive and collar post testing whilst minimising the risk of damage to the cell wall. This test arrangement resulted in a combined additional weight of approximately 2.6 g (circa: 6% additional mass for each cell). Their inclusion within the experimental set-up was not deemed to have any significant impact on test accuracy through the addition of increased mass. When the cells were installed, the collars were levelled using a digital inclinometer. This was to ensure that no "off axis" errors would occur. Two control accelerometers (model PCB 352A24) were secured at opposite ends of the test fixture, but close to the specimens (as shown in Fig. 15) using petro-wax.

An averaging strategy of the control accelerometers was employed during the natural frequency measurement. Data was recorded at 2.5 times the desired peak frequency in accordance with Niquest rate guidelines. Each sweep was performed three times and an average response was recorded.

2.6. Application of vibration

The vibration profiles, discussed within Section 2.4 were applied to the cells (sample numbers 1–9) in 6 DOF for 150 h in accordance with the surface repeats defined in Table 6. The cells

Table 8
Change in Pulse Power Performance – DC Resistance.

Cell ID	Orientation	DC Resistance (SOT) (mΩ)	DC Resistance (EOT) (mΩ)	Change in DC Resistance (mΩ)	Percentage Change in DC Resistance Difference Between SOT and EOT (%)	Ranking Worst to Best: 1 = Worst, 9 = Best
1	Z	40.56	43.51	2.95	7.28	3
2	Z	40.82	43.80	2.98	7.31	2
3	Z	40.64	43.33	2.69	6.62	5
4	Y	41.08	43.36	2.28	5.55	8
5	Y	40.91	43.45	2.54	6.22	7
6	Y	40.38	43.13	2.75	6.81	4
7	X	41.32	43.95	2.63	6.37	6
8	X	40.00	43.51	3.51	8.77	1
9	X	41.32	43.42	2.11	5.10	9
10	Control	41.90	42.98	1.08	2.58	–
11	Control	42.22	42.92	0.70	1.66	–
12	Control	41.37	42.66	1.29	3.11	–

Pulse Power – Mean Change

	Mean Change (mΩ)	Mean Change (%)	Ranking
Mean Change in Pulse Power DC Resistance (mΩ) – X	2.75	6.75	2
Mean Change in Pulse Power DC Resistance (mΩ) – Y	2.52	6.19	3
Mean Change in Pulse Power DC Resistance (mΩ) – Z	2.88	7.07	1
Mean Change in Pulse Power DC Resistance (mΩ) – Control	1.02	2.45	–

Pulse Power – ANOVA Analysis

Orientation	ANOVA p-value against Control Null Hypothesis: Mean of vibrated cells and control cells are equal. Reject null hypothesis if $p < 0.05$)
X	0.018
Y	0.002
Z	0.001

were checked every 4 h for any significant changes in temperature or any emission of gases via the remote monitoring systems, as discussed in 2.2.2.

2.7. Electrochemical characterisation after the application of vibration

At the end of the 150 h durability vibration profile, the cells were left to rest for 4 h prior to visual inspection. EOT characterisation of the cells, both in terms of the electrical performance and mechanical attributes was then conducted by repeating the tests defined in Section 2.5.

3. Cell degradation results

The following section introduces the data to quantify the electromechanical attributes for all cells (sample numbers 1–12) at SOT and EOT. Trends in the measurements are made for testing of the NCA 18650 cells subject to 150 h of vibration in 6DOF. A discussion is presented that highlights the effect of vibration on cell performance and identifies if cell orientation can impact vibration robustness.

3.1. Post test external condition of cells through visual inspection

Post testing, no significant mechanical damage or degradation was observed in any of the test samples, this included no leaking or expulsion of electrolyte was witnessed.

3.2. Estimation of DC resistance through pulse power measurements

All samples illustrated an increase in resistance post vibration testing. Table 8 illustrates the change in estimated DC resistance from the pulse power test (PPT) for all samples (including control samples). Based on established methods of benchmarking laboratory processes and facilities, the experimental error associated with pulse power DC resistance estimation on 18650 cells is $\pm 0.53\,m\Omega$ [48]. Whilst the standard error (e.g. the confidence in the sample mean resulting from the experiment due to past confidence with the experiment and cell-type) is 0.62% [48].

From Table 3, the worst performing cell was sample 8 (orientated along the X-axis) which shows an 8.77% increase in DC resistance. The cell with the least degradation in DC resistance post vibration was sample 9 (orientated along the X-axis) which has a 5.10% increase. With all samples subject to vibration, an increase in pulse power resistance was observed which potentially indicates a decrease in current collector contact area, possibly as a result of delamination or cracking of internal electrode surfaces [21]. A mean increase in DC resistance of 2.45% was observed within the control samples compared to a mean of 7.07%, 6.19% and 6.75% for the Z, Y and X oriented samples respectively. This suggests that vibration has a statistically significant effect on the cell performance. This is confirmed by the analysis of variance (ANOVA) presented in Table 8. Based on the ANOVA analysis the following hierarchy of orientation related performance is determined from these results at the 95% confidence level: $Y < X < Z$.

3.3. EIS results

Tables 9 and 10 show the ohmic resistance (R_O) and the charge transfer resistance (R_{CT}) of the cells at SOT and EOT. A complete interpretation of EIS results is beyond the scope of this study, but is discussed within [49,50] for reference. By means of an example, Fig. 16 presents the Nyquist plot of sample 4, before and after the application of the vibration durability test.

The results illustrate the typical characteristics of the cell captured by the EIS measurement. Table 9 highlights that all cells, including the control samples, exhibit an increase in R_O at EOT. Sample 6 (orientated along the Y-axis) exhibits the greatest change in R_O of $2.12\,m\Omega$ (9.39%). However, sample 4 which was also orientated in the Y axis exhibited the least change in R_O of $0.99\,m\Omega$ (4.20%). An increase in R_o typically originates from an increase in cell contact resistance, possibly through delamination of the material layers [49,50] or due to damage within the current collectors. However, the mean change in Ro resistance for the control samples is $1.59\,m\Omega$ (6.92%), compared to $1.57\,m\Omega$ (6.89%),

Table 9
Start and End of Test – R_o Measurements.

Cell ID	Orientation	SOT (mΩ)	EOT (mΩ)	Change from SOT and EOT (mΩ)	Percentage Change (%)	Overall Ranking: 1 = Worst, 9 = Best
1	Z	22.99	24.45	1.47	6.39	4
2	Z	23.12	24.90	1.78	7.68	3
3	Z	23.26	24.60	1.34	5.78	6
4	Y	23.57	24.56	0.99	4.20	9
5	Y	23.25	24.61	1.35	5.82	5
6	Y	22.58	24.70	2.12	9.39	1
7	X	23.24	24.57	1.33	5.74	7
8	X	22.35	24.43	2.09	9.33	2
9	X	23.23	24.54	1.31	5.62	8
10	Control	22.66	24.12	1.45	6.41	–
11	Control	23.27	24.89	1.62	6.96	–
12	Control	22.77	24.46	1.69	7.41	–

R_O – Mean Change

	Mean Change (mΩ)	Mean Change (%)	Ranking
Mean Change in R_O (mΩ) – X	1.57	6.89	1
Mean Change in R_O (mΩ) – Y	1.49	6.47	3
Mean Change in R_O (mΩ) – Z	1.53	6.62	2
Mean Change in R_O (mΩ) – Control	1.59	6.93	–

R_O – ANOVA Analysis

Orientation	ANOVA p-value against Control Null Hypothesis: Mean of vibrated cells and control cells are equal. Reject null hypothesis if $p < 0.05$)
X	0.967
Y	0.786
Z	0.718

Table 10
Start and End of Test R_{CT} Measurements – Items in Italics Indicate a Reduction in R_{CT}.

Cell ID	Orientation	SOT (mΩ)	EOT (mΩ)	Change from SOT and EOT (mΩ)	Percentage Change (%)	Overall Ranking: 1 = Worst, 9 = Best
1	Z	14.38	11.44	*−2.94*	*−20.47*	6
2	Z	15.64	13.97	*−1.67*	*−10.68*	4
3	Z	15.64	13.88	*−1.76*	*−11.24*	5
4	Y	16.57	12.79	*−3.78*	*−22.83*	7
5	Y	17.42	12.04	*−5.38*	*−30.86*	9
6	Y	16.46	12.52	*−3.95*	*−23.99*	8
7	X	12.26	12.38	0.12	0.95	1
8	X	13.73	12.50	*−1.24*	*−9.01*	3
9	X	17.33	16.67	*−0.66*	*−3.79*	2
10	Control	21.31	16.27	*−5.04*	*−23.64*	–
11	Control	22.25	14.62	*−7.63*	*−34.31*	–
12	Control	19.03	16.20	*−2.83*	*−14.86*	–

R_{CT} – Mean Change

	Mean Change (mΩ)	Mean Change (%)	Ranking
Mean Change in R_{CT} (mΩ) – X	*−0.59*	*−3.95*	1
Mean Change in R_{CT} (mΩ) – Y	*−4.37*	*−25.89*	3
Mean Change in R_{CT} (mΩ) – Z	*−2.12*	*−14.13*	2
Mean Change in R_{CT} (mΩ) – Control	*−5.17*	*−24.27*	–

R_{CT} – ANOVA Analysis

Orientation	ANOVA p-value against Control Null Hypothesis: Mean of vibrated cells and control cells are equal. Reject null hypothesis if $p < 0.05$)
X	0.033
Y	0.618
Z	0.103

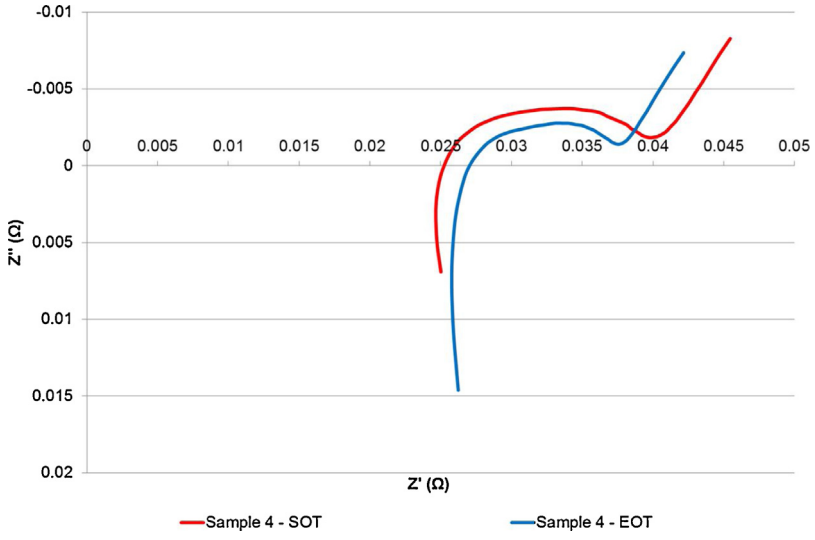

Fig. 16. Typical Pre and Post Test EIS Curves for Test Samples.

1.49 mΩ (6.47%) and 1.53 mΩ (6.62%) for the X, Y and Z orientations respectively. This indicates that whilst vibration may have had an effect on this electromechanical property, it is not possible to isolate the level degradation observed from other ageing mechanisms, for example those associated with cell storage. ANOVA analysis of the significance of the mean change in ohmic resistance of the tested cells in relation to the control samples is shown in Table 9. Based on this statistical analysis, there is no significant change in R_O for any of the three cell orientations at the 95% confidence level as a result of the application of vibration in 6DOF.

The R_{CT} results presented in Table 10 demonstrate that all samples (except sample 7), including the control samples, show a decrease in R_{CT} post testing.

This reduction in R_{CT} could be a function of improved anode and cathode "wetting" over the duration of the test [51]. However, given that the control samples display a similar improvement, this proposed mechanism is unlikely to be as a function of applied vibration. Samples evaluated in the Y orientation show a similar average reduction in R_{CT} as the control samples. They also have a significantly higher mean change of −25.89% than the X axis oriented items (−3.95%). The Z-axis oriented samples have a lower improvement to that of the Y oriented samples and the controls of −14.13%. Reviewing the ANOVA analysis results presented in Table 10, samples mounted in the X axis orientation show a significant difference in R_{CT} as a result of vibration when compared to the control samples. It is noteworthy that R_{CT} has reduced in all samples post vibration testing. The reduction was lower in X axis

orientated samples, resulting in a significant effect of vibration within these samples. In summary, assessing the mean change with regard to R_{CT}, the performance of cell orientation can be summarised as follows: Y = Z < X.

3.4. OCV measurement

No statistically significant changes in the OCV measurements were observed between SOT and EOT. Typically, a change of −0.026% to −0.05% was observed. As discussed within Section 3.2, this difference is within the error limits of the measurement method. These results support those presented in [22,23] that also noted that OCV is not adversely affected by vibration loading. Due to the level of change, the OCV results and ANOVA analysis have been omitted from this paper. However, no significant change in OCV, as a result of vibration, was observed at the 95% confidence level between cell samples 1–9 and the control cells (samples 10–12).

3.5. 1C discharge capacity results

All samples, including the control samples, illustrate a reduction in 1C capacity post vibration testing. The results from the 1C discharge evaluation are shown in Table 11. It is evident from these results that the reduction in capacity observed in the control samples is greater than that observed within samples 1–9. This is also evident when viewing the mean change in cell capacity of each cell orientation is compared to the mean of the control samples. Interestingly the ANOVA analysis of the Y axis samples indicates that there is a statistically significant change in capacity performance as a result of vibration. However, this is due to the greater reduction of 1C capacity observed in the control samples as opposed to the direct effect of vibration loading.

3.6. C/3 discharge capacity results

In a similar manner to the 1C capacity discharge results discussed in 3.5 all samples, including the control cells, display a reduction in C/3 capacity measurement post vibration durability testing. This is illustrated in Table 12. A noteworthy observation is that the C/3 performance of the Y axis samples is, on average, the worst performing orientation. This is likely to be as a result of sample 6 which has a higher level of capacity reduction (−4.22%).

The control samples also exhibit a higher reduction in capacity at EOT. This indicates that from a capacity reduction perspective there may be some evidence to suggest that cells excited to vibration in 6DOF may degrade at a slower rate than cells left in a static condition. However, it must be noted that further testing is required to confirm this hypothesis. The ANOVA analysis presented in Table 12, highlights that there is no significant effect to C/3 capacity for any of the orientations as a result of vibration in 6DOF.

3.7. Resonance search via swept sine results

No change in natural frequency between the SOT and EOT was observed. Whilst it is likely that no significant mechanical degradation occurred which could have affected the natural frequency, it is noteworthy that the resonance of the cells was greater than the frequency range capabilities of the EMS table which was used for the natural frequency measurement. Subsequently the first natural frequency of all samples has been recorded as 3700 Hz within Table 13.

With regard to the amplitude of the *first resonant frequency* (which was recorded as 3700 Hz) as shown in Table 14, there is a significant change in the majority of cells indicating a change in damping within the cell assembly. The greatest change in amplitude was observed within sample 6 (Y-axis), which had an increase of 39.22%, highlighting a reduction in cell damping. Generally, Y axis oriented cells exhibit a greater reduction in

Table 11
Ranked Change in Capacity of All Cells – Items in Italics Indicate a Reduction in Capacity.

Cell ID	Orientation	SOT (Ah)	EOT (Ah)	Change from SOT and EOT (Ah)	Percentage Change (%)	Overall Ranking: 1 = Worst, 9 = Best
1	Z	2.97	2.88	*−0.09*	*−3.03*	1
2	Z	2.98	2.90	*−0.08*	*−2.68*	5
3	Z	2.94	2.92	*−0.02*	*−0.68*	=9
4	Y	2.98	2.91	*−0.07*	*−2.35*	6
5	Y	2.97	2.94	*−0.03*	*−1.01*	7
6	Y	3.01	2.92	*−0.09*	*−2.99*	3
7	X	2.95	2.87	*−0.08*	*−2.71*	4
8	X	2.99	2.90	*−0.09*	*−3.01*	2
9	X	2.94	2.92	*−0.02*	*−0.68*	=9
10	Control	3.06	2.92	*−0.14*	*−4.58*	–
11	Control	3.08	2.94	*−0.14*	*−4.55*	–
12	Control	3.07	2.97	*−0.10*	*−3.26*	–

Mean Change – 1C Discharge

	Mean Change (mΩ)	Mean Change (%)	Ranking
Mean Change in (Ah) – X	*−0.06*	*−2.13*	=1
Mean Change in (Ah) – Y	*−0.06*	*−2.12*	2
Mean Change in (Ah) – Z	*−0.06*	*−2.13*	=1
Mean Change in (Ah) – Control	*−0.13*	*−4.13*	–

ANOVA Analysis – 1C Discharge

Orientation	ANOVA p-value against Control Null Hypothesis: Mean of vibrated cells and control cells are equal. Reject null hypothesis if $p < 0.05$)
X	0.0687
Y	0.0457
Z	0.0687

Table 12
Ranked Change in C/3 Capacity of All Cells – Items in Italic Indicate a Reduction in Capacity.

Cell ID	Orientation	SOT (Ah)	EOT (Ah)	Change from SOT and EOT (Ah)	Percentage Change (%)	Overall Ranking: 1 = Worst, 9 = Best
1	Z	2.98	2.90	*−0.08*	*−2.68*	3
2	Z	3.03	2.95	*−0.08*	*−2.64*	4
3	Z	3.03	2.98	*−0.05*	*−1.65*	7
4	Y	2.98	2.92	*−0.06*	*−2.01*	5
5	Y	3.02	2.97	*−0.05*	*−1.66*	6
6	Y	3.08	2.95	*−0.13*	*−4.22*	2
7	X	2.91	2.88	*−0.03*	*−1.03*	8
8	X	3.07	2.93	*−0.14*	*−4.56*	1
9	X	2.95	2.92	*−0.03*	*−1.02*	9
10	Control	3.02	2.90	*−0.12*	*−3.97*	–
11	Control	3.09	2.94	*−0.15*	*−4.85*	–
12	Control	3.04	3.01	*−0.03*	*−0.99*	–

Mean Change – C/3 Discharge

	Mean Change (mΩ)	Mean Change (%)	Ranking
Mean Change in (Ah) – X	*−0.07*	*−2.20*	3
Mean Change in (Ah) – Y	*−0.08*	*−2.63*	1
Mean Change in (Ah) – Z	*−0.07*	*−2.32*	2
Mean Change in (Ah) – Control	*−0.10*	*−3.27*	–

ANOVA Analysis – C/3 Discharge

Orientation	ANOVA p-value against Control Null Hypothesis: Mean of vibrated cells and control cells are equal. Reject null hypothesis if $p < 0.05$)
X	0.552
Y	0.673
Z	0.468

Table 13
Summary of Change in Natural Frequency of Observed First Cell Resonance.

		First Resonance Frequency (Hz)				
ISR number	Orientation	SOT	EOT	Change	Change (%)	Ranking: 1 = Worst, 9 = Best
1	Z	3700	3700	0.00	0.00	=
2	Z	3700	3700	0.00	0.00	=
3	Z	3700	3700	0.00	0.00	=
4	Y	3700	3700	0.00	0.00	=
5	Y	3700	3700	0.00	0.00	=
6	Y	3700	3700	0.00	0.00	=
7	X	3700	3700	0.00	0.00	=
8	X	3700	3700	0.00	0.00	=
9	X	3700	3700	0.00	0.00	=

	Mean Change (Hz)	Mean Change (%)	Ranking
Mean Change First Resonance Frequency – X	0.00	0.00	=
Mean Change First Resonance Frequency – Y	0.00	0.00	=
Mean Change First Resonance Frequency – Z	0.00	0.00	=

damping than other cell orientations. This observation could be due to a redistribution of electrolyte within the cell's material layers due to vibration. However, further studies must be conducted to determine the underpinning reason. Assessing the mean change with regard to the amplitude of the first natural frequency, the performance of cell orientation can be summarised as follows: X < Z < Y. ANOVA analysis could not be performed for the mechanical characterisation results, because as discussed in Section 2.1 the control samples were not subject to a resonance search.

Table 15 presents the post-test dimensions of the cells when compared to the change in amplitude of the peak natural frequency measured. A noteworthy observation is that cells with a longer length typically have a greater change of amplitude between the start and end of test. Another observation is that the lengths of samples 1, 3, 4 and 8 are outside the manufacturer's tolerance of maximum length tolerance of 65.3 mm.

4. Discussion

4.1. Effect of vibration in 6 DOF on 18650 NCA Li-ion cells

The primary conclusion from this study is that both the electrical performance and the mechanical properties of the NCA Li-ion cells employed are relatively unaffected when exposed to vibration energy that is commensurate with a typical vehicle life. However, there are some nuances within the data that are worthy of further discussion.

4.1.1. The impact of vibration on electrical cell performance

It's noticeable from the ANOVA analysis in Section 3.2 (Table 8) that the value of R_{DC} was significantly impacted by vibration applied in 6DOF when compared to the control samples. This indicates that the cells may have some degree of damage to the

Table 14
Summary of Change in Amplitude of Observed First Cell Resonance.

		Amplitude at First Resonance (g_n)				
Sample number	Orientation	SOT	EOT	Change	Change (%)	Ranking: 1 = Worst, 9 = Best
1	Z	1.66	1.82	0.16	9.64	4
2	Z	1.61	1.68	0.07	4.35	8
3	Z	1.70	1.81	0.11	6.47	6
4	Y	1.80	1.97	0.17	9.44	5
5	Y	1.70	2.24	0.54	31.76	2
6	Y	2.04	2.84	0.80	39.22	1
7	X	1.70	1.78	0.08	4.71	7
8	X	1.54	1.70	0.16	10.39	3
9	X	1.89	1.90	0.01	0.53	9

	Mean Change (g_n)	Mean Change (%)	Ranking
Mean Change in Amplitude in First Resonance – X	0.08	5.21	3
Mean Change in Amplitude in First Resonance – Y	0.50	26.81	1
Mean Change in Amplitude in First Resonance – Z	0.11	6.82	2

Table 15
Dimensions of Cells Post Testing in Relation to Change in Amplitude.

Sample number	Positive End of Cell Diameter (mm)	Negative End of Cell Diameter (mm)	Length of Cell (mm)	Positive End of Cell Diameter Ranking: Biggest = 1, Smallest = 9	Negative End of Cell Ranking: Biggest = 1, Smallest = 9	Length of Cell: Biggest = 1, Smallest = 9	Change in Amplitude Ranking: Worst = 1, Best = 9
1	17.96	18.20	65.65	4	1	1	4
2	17.92	18.03	65.24	9	9	8	8
3	17.94	18.13	65.35	6	4	4	6
4	17.99	18.11	65.44	1	6	2	5
5	17.97	18.08	65.26	2	7	6	2
6	17.93	18.17	65.28	8	2	5	1
7	17.96	18.08	65.25	5	8	7	7
8	17.94	18.12	65.40	7	5	3	3
9	17.97	18.14	65.16	3	3	9	9

current collector or cell material layers as a result of the multi-axis vibration loading. However, this finding is not confirmed by the degree of change observed with the measurement of $R_{O.}$ Like R_{DC}, R_O is also taken within some studies as an indication of current collector condition and material layer integrity [52,53]. Whilst there is degradation within the observed average values for each orientation, the difference between the control and tested items is minimal. This limited difference between the control and tested items implies that vibration is the non-significant contributor to the increase in $R_{O.}$ To better understand what may be occurring within these cells further testing via non-destructive methods (such as computer tomography (CT) scanning) followed by chemical and microscopic analysis of the cell layers may be employed. Example test methods that may be appropriate are discussed further within [21].

Another observation with respect to the change in R_{DC}, R_O and also capacity (both 1C and C/3) show a relatively linear degradation post testing regardless of cell orientation. In previous results published within [13,28] there has been a significant difference in the performance of different cell orientations. However, unlike previous studies (where cells have had a separate vibration profile applied for each vehicle axis and the cells have been subsequently rotated on a rig to achieve the correct loading), this study has applied the vibration in a more representative manner where all

Table 16
Comparison of Cell Performance Ranking by Post Test Assessment.

		Electrical Characterisation						Mechanical Characterisation	
Cell	Orientation	Pulse Power Results Ranking	EIS Results Ranking R_o	EIS Results Ranking R_{CT}	OCV Results Ranking	Capacity Results Ranking 1C	Capacity Results Ranking C/3	Resonance Results – Frequency Ranking	Resonance Results – Amplitude Ranking
1*	Z	3	4	6	No change	5	3	No change	4
2	Z	2	3	4	No change	3	4	No change	8
3*	Z	5	6	5	No change	8	7	No change	6
4*	Y	8	9	7	No change	3	5	No change	5
5	Y	7	5	9	No change	5	6	No change	2
6	Y	4	1	8	No change	1	2	No change	1
7	X	6	7	1	No change	7	8	No change	7
8*	X	1	2	3	No change	2	1	No change	3
9	X	9	8	2	No change	8	9	No change	9

Note: 1 = Worst performing, 9 = Best performing, * = Sample with length greater than manufacturers maximum stated length.

Table 17
Assessment Ranking of Orientation by Test.

Assessment	Test	Orientation Ranking By Assessment		
		Least Change	⇨	Greatest Change
Electrical Characterisation				
Pulse Power	6DOF	Y	X	Z
EIS (Ro)	6DOF	X = Y = Z		
EIS (R_{CT})	6DOF	Y = Z		X
OCV	6DOF	X = Y = Z		
Capacity – 1C Discharge	6DOF	Y	Z = X	
Capacity – C/3 Discharge	6DOF	X = Y = Z		
Mechanical Characterisation				
Resonance (Change in Frequency)	6DOF	X = Y = Z		
Resonance (Change in Amplitude)	6DOF	X	Z	Y

degrees of motion are applied simultaneously. An interesting observation from this study is the decrease in R_{CT}. As discussed in Section 3.3, given that the control samples have not displayed a significant decrease, it is unlikely that this reduction is a result of vibration. As observed within [13,28] the OCV shows no significant change post testing regardless of changes to the other measured attributes.

4.1.2. The impact of vibration on mechanical cell performance

For the mechanical characterisation of the cells, none of the cells showed a significant change in natural frequency. This supports the general finding of the electrical characterisation data, indicating that vibration has had a minimal impact on cell performance. However, as highlighted in Section 3.7, the natural frequency of the cells was outside the capability of the shaker table used for the natural frequency assessment. With regard to the change of amplitude of the cells it is noteworthy that a change in damping was observed indicating some change in the structural stiffness may have occurred.

4.1.3. Summary of EOT electrical and mechanical test results

Table 16 shows the ranked performance of each cell from the eight sets of characterisation data. Interestingly within this study there is some evidence of consistently poor performing cells when ranked per test. For example, sample 9 (tested in the X orientation) is typically one of the best performing cells for all assessments. Conversely sample 6 (subject to vibration in the Y orientation) generally is the worst performing cell. There is also some correlation between the electrical characterisation performance and the change in resonance amplitude which has not been witnessed in any of the previous 18650 cell vibration durability studies [13,28]. There are several possible factors for the increase in the observed correlation within this test between electrical and mechanical characterisation methods. Firstly, the vibration signals within this study are a replication of actual EV battery measurements in the time domain. The vibration spectra within [13,28] is applied in a random nature within given spectral parameters may result in a greater variation in level degradation observed. Secondly, the test items within this study are evaluated with respect to gravity. Within [13,28] a single axis vertical shaker was used and the samples were rotated on the fixture to achieve the desired loading. Whilst this is industry practice, the process may result in unrepresentative loading as the effect of gravity is not considered [29].

With respect to orientation within the vehicle, Table 17 presents a summary of each assessment's results', for each packaging axis. The data illustrated in Table 17 suggests that there is no clear overriding orientation that is consistently worse with respect to cell degradation. What is noticeable from this tabulated data set is that the effect is equal in a large proportion of the performance tests. This indicates that the cells are potentially robust to differences of in-vehicle packaging orientation.

4.1.4. Implications for vehicle design

Whilst the cells evaluated within this study were typically unaffected by road vibration excitation representative of 10 year life, there were some specific aging behaviour such as the statistical significant increase in DC resistance (derived from pulse power testing) observed. Any aging behaviour as a function of vibration would have to be characterized to ensure effective battery management system (BMS) development, to maximize useful service life and to minimise potential warranty related issues.

The test methodology presented within this paper allows engineers to determine how susceptible a proposed cell technology is to vibration. Furthermore, the underpinning methodology within this paper could also be applied to other chassis mounted electrical components within the battery assembly, such as contactors, bus bars, relays, electrical control units and power electronic devices.

5. Further Work

Whilst this study shows that vibration has a limited effect on the performance of the commercially available 18650 NCA cells employed, it would be beneficial to test other cell chemistries, form-factors and module systems using the same methodology to determine their robustness to mechanical excitation. This would highlight the transferability of these results to other technologies employed within the EV sector. One of the limitations of the methodology employed within this study is that electrical and mechanical characterisation data was only measured at SOT and EOT. As a result, no discussion or conclusions can be made about the rate of degradation that may be observed throughout the vehicle's life. Whilst it can be concluded from this study that no significant degradation was observed, this may not be the case for other technologies. It is therefore recommended that future studies should characterise the cells at intermediate points during the test programme, e.g. intervals representative of 10,000 miles or for each year of vehicle use. This would facilitate further investigation into both the absolute value of degradation, but also the expected in-service rate of performance reduction. This study recommends that an alternative method of natural frequency measurement of 18650 cells is investigated. Candidate methods include modal analysis via Laser Doppler Vibrometer measurement techniques, such as those discussed within [54,55]

or through the use of a smaller single axis shaker with a higher peak frequency capability. This would allow the validation of the cells in a free–free condition, both pre and post testing. This would ensure the effects of the fixture could be eliminated from the analysis and would allow for the identification of mode shapes of the test item.

6. Conclusions

Both the electrical performance and the mechanical properties of the commercially available NCA 18650 Li-ion cell employed in this study typically showed no statistically significant degradation as a result of vibration applied in 6DOF. Furthermore, no particular cell orientation consistently displayed a significantly greater reduction in cell performance or a significant change in cell mechanical properties. Within the context of this study, cell characterisation within the electrical domain was done through quantification of the cell's impedance, the open-circuit potential and the cell's energy capacity. A statistically significant change in R_{DC} was observed post vibration testing on all NCA 18650's for all three cell orientations. The orientation with the greatest susceptibility to a change in R_{DC} as a result of vibration in 6DOF was the Z axis. The remainder of electrical attributes employed to characterise cell performance all indicate either no statistically significant change or a reduction in performance that may not be attributed directly to vibration loading of the cell. The mechanical properties of the cell were inferred through measurement of the cell's natural frequency of vibration and the associated damping ratio and stiffness. With regard to mechanical integrity, no significant external damage or electrolyte leakage was observed in any of the tested cells post vibration. No change in sample natural frequency was observed. However, samples oriented in the Y axis displayed a significant reduction in natural frequency amplitude post vibration indicating a possible change in cell stiffness. Within this study there was a degree of correlation between cell natural frequency amplitude and a change in the cells' electrical performance. In conclusion, the results presented in this paper highlight that this particular cell design, one that is already being used or investigated by many leading vehicle manufacturers, is largely robust to vibration excitation that is commensurate with a typical 10-year vehicle life.

Acknowledgements

The research presented within this paper is supported by the Engineering and Physical Science Research Council (EPSRC – EP/I01585X/1) through the Engineering Doctoral Centre in High Value, Low Environmental Impact Manufacturing. The research was undertaken in collaboration with the Warwick Manufacturing Group (WMG) Centre High Value Manufacturing Catapult (funded by Innovate UK) and Jaguar Land Rover. The authors would like to express their gratitude to Millbrook Proving Ground Ltd (Component Test Laboratory) for their support and advice throughout the test program.

References

[1] A. Dasgupta, C. Choi, E. Habtour, Simulation and test vibration-nonlinear dynamic effects in vibration durability of electronic systems, 8th International Conference on Integrated Power Systems, University of Maryland, College Park, MD 20742, USA: Nuremberg, Germany, 2014.
[2] J. Hooper, J. Marco, Defining a representative vibration durability test for electric vehicle (EV) rechargeable energy storage systems (RESS), Electric Vehicle Show 29 (EVS29), Montreal, Canada, 2016 p. 1–6.
[3] A. Halfpenny, Methods for accelerating dynamic durability tests, 9th International Conference in the Advances in Structural Dynamics, nCode, Southampton, England, 2006 p. 1–19.
[4] S.-I. Moon, I.-J. Cho, D. Yoon, Fatigue life evaluation of mechanical components using vibration fatigue analysis technique, J. Mech. Sci. Technol. 25 (3) (2011) 611–637.
[5] M. Firat, U. Kocabicak, Analytical durability modeling and evaluation—complementary techniques for physical testing of automotive components, Eng. Fail. Anal. 11 (2004) 655–674.
[6] A. Halfpenny, Methods for accelerating dynamic durability tests, 9th International Conference on Recent Advances in Structural Dynamics, Southampton, 2006, pp. 1–19.
[7] A. Vertua, A. Halfpenny, F. Kihm, Proving ground optimisation based on fatigue damage spectra, in French Society for Metallurgy and Materials – SF2M, Journées de Printemps 2011 (2011) 1–13 nCode.
[8] K. Muniyasamy, R. Govindarajan, N. Jayaram, R. Kharul, Vibration fatigue analysis of motorcycle front fender (2005-32-0030), SAE Int. 1 (2005) 1–5.
[9] P.D. Rawlinson, in: T.M. Pack (Ed.), Integration System for a Vehicle Battery, Tesla Motors Inc., 2012, pp. 1–21.
[10] S. Arora, W. Shen, A. Kapoor, Review of mechanical design and strategic placement technique of a robust battery pack for electric vehicles, Renew. Sustain. Energy Rev. 60 (2016) 1319–1331.
[11] B. Nykvist, M. Nilsson, Rapidly falling costs of battery packs for electric vehicles, Nat. Clim. Change 5 (2015) 329–332.
[12] L. Huat Saw, Y. Ye, A.A.O. Tay, Integration issues of lithium-ion battery into electric vehicles battery pack, J. Clean. Prod. 113 (2016) 1032–1045.
[13] J. Hooper, J. Marco, G. Chouchelamane, C. Lyness, Vibration durability testing of nickel manganese cobalt oxide (NMC) lithium-ion 18650 battery cells, Energies 9 (52) (2016) 27.
[14] United Nations, Transport of Dangerous Goods – Manual of Tests and Criteria – Fifth Edition – Amendment 1, United Nations, New York, 2011, pp. 62.
[15] United Nations, ECE R100—Battery Electric Vehicles with Regard to Specific Requirements for the Construction, Functional Safety and Hydrogen, United Nations, 2002.
[16] I. Avdeev, M. Gilaki, Structural analysis and experimental characterization of cylindrical lithium-ion battery cells subject to lateral impact, J. Power Sources 271 (2014) 382–391.
[17] L. Greve, C. Fehrenbach, Mechanical testing and macro-mechanical finite element simulation of the deformation, fracture, and short circuit initiation of cylindrical lithium-ion battery cells, J. Power Sources 214 (2012) 377–385.
[18] E. Sahraei, J. Meiera, T. Wierzbicki, Characterizing and modeling mechanical properties and onset of short circuit for three types of lithium-ion pouch cells, J. Power Sources 247 (2014) 503–516.
[19] X. Feng, J. Sun, M. Ouyang, F. Wang, X. He, L. Lu, H. Peng, Characterization of penetration induced thermal runaway propagation process within a large format lithium-ion battery module, J. Power Sources 275 (2015) 261–273.
[20] H.Y. Choi, J.S. Lee, Y.M. Kim, H. Kim, A Study on Mechanical Characteristics of Lithium-Polymer Pouch Cell Battery for Electric Vehicle, Hongik University, Seoul, South Korea, 2013 p. 1–10.
[21] M. Brand, S. Schuster, T. Bach, E. Fleder, M. Stelz, S. Glaser, J. Muller, G. Sextl, A. Jossen, Effects of vibrations and shocks on lithium-ion cells, J. Power Sources 288 (2015) 62–69.
[22] J.T. Chapin, W. Alvin, W. Carl, Study of Aging Effects on Safety of 18650-Type LiCoOx Cells, Underwriters Laboratory Inc., Northbrook, Illinois, US, 2011.
[23] A. Wu, Study on Aging Effects on Safety of 18650 Type LICOOX Cells, Product Safety Engineering Society/UL, 2017.
[24] P. Svens, Methods for Testing and Analyzing Lithium-Ion Battery Cells Intended for Heavy-Duty Hybrid Electric Vehicles, in Department of Chemical Engineering and Technology, KTH Royal Institute of Technology, Stockholm, Sweden, 2014 p. 87.
[25] D. Pohl, Lithium iron phospahate: what factors influence the durability of storage systems, in: A. Levran (Ed.), Solar Energy Storage, 2014.
[26] A. Suttman, Lithium Ion Battery Aging Experiments and Algorithm Development for Life Estimation, The Ohio State University, Ohio, USA, 2011 p. 122.
[27] T. Harrison, An Introduction to Vibration Testing, Bruel and Kjaer Sound and Vibration Measurement, Naerum, Denmark, 2014 11.
[28] J. Hooper, J. Marco, G. Chouchelamane, C. Lyness, J. Taylor, Vibration durability testing of nickel cobalt aluminum oxide (NCA) lithium-ion 18650 battery cells, Energies 9 (281) (2016) 1–18.
[29] W. Tustin, Sumultaneous multiple axis vibration testing, The AMMTIAC Q. 3 (4) (2016) 13–14.
[30] C.-J. Kim, Y.J. Kang, B.-H. Lee, Generation of driving profile on a multi-axial vibration table for vibration fatigue testing, Mech. Syst. Sig. Process. 26 (2012) 244–253.
[31] E. Habtour, W. Connon, M. Pohland, S. Stanton, M. Paulus, A. Dasgupta, Review of response and damage of linear and nonlinear systems under multiaxial vibration, Shock Vib. 2014 (2014) 1–21.
[32] M. Ernst, E. Habtour, A. Dasgupta, M. Pohland, M. Robeson, M. Paulus, Comparison of electronic component durability under uniaxial and multiaxial random vibrations, J. Electron. Packag. 137 (2015) 011009-1–011009-8.
[33] M. Ecker, N. Nieto, S. Käbitz, J. Schmalstieg, H. Blanke, A. Warnecke, D. Uwe Sauer, Calendar and cycle life study of Li(NiMnCo)O2-based 18650 lithium-ion batteries, J. Power Sources 248 (2014) 839–851.
[34] Q. Zhang, R.E. White, Calendar life study of Li-ion pouch cells, J. Power Sources 173 (2007) 990–997.
[35] K. Buckley, L. Chiang, Design and Analysis of Vibration Test Fixtures for Payloads, Worcester Polytechnic Institute, Worcester, MA, USA, 2010 p. 107.

[36] Srinivas Reddy, Vijaya Kumar Reddy, Design and analysis of vibration test bed fixtures for space launch vehicles, Indian J. Sci. Technol. 5 (6) (2010) 592–595.
[37] Fixtures for B&K Exciters, Bruel Kjaer, Naerum, Denmark, 1987 p. 1–24.
[38] T. Harrison, Resonance. Vibration Testing, vol. 5, Bruel and Kjaer, Naerum, Denmark, 2014 11.
[39] T. Harrison, A Practical Guide to Vibration Testing, Brüel & Kjær Royston, Hertfordshire, 2014 p. 11.
[40] British Standards, BS EN 60068 Environmental Testing, British Standards, 2017.
[41] P. Avitabile, Experimental modal analysis—a simple non-mathematical presentation, Sound Vib. (January) (2001) 3–11.
[42] J. Hooper, J. Marco, Experimental modal analysis of lithium-ion pouch cells, J. Power Sources 285 (2015) (2015) 247–259.
[43] G. Kerschen, J.-C. Golinval, Experimental Modal Analysis, UNIVERSITÉ DE LIÈGE, Liege, Belgium, 2010 p. 24.
[44] A. Burgess, Transient Response of Mechanical Structures Using Modal Analysis Techniques, in Department of Mechanical Engineering, Imperial College London, London, 1988.
[45] J. Hooper, J. Marco, Characterising the in-Vehicle vibration inputs to the high voltage battery of an electric vehicle, J. Power Sources 245 (2014) 510–519.
[46] J. Hooper, J. Marco, Understanding vibration frequencies experienced by electric vehicle batteries, HEVC 2013-4th Hybrid and Electric Vehicles Conference, IET, London, England, 2013 p. 1–6.
[47] Millbrook Proving Ground, Millbrook Structural Durability Procedure, Millbrook Proving Ground, Millbrook, Bedfordshire, England, 2012.
[48] J. Taylor, in: J. Hooper (Ed.), Uncertainty/Error Measurement of Electrical Characterisation Methods, WMG: WMG, University of Warwick, Coventry, CV4 7AL, 2015 p. 1–3.
[49] A. Barai, G.H. Chouchelamane, Y. Guo, A. McGordon, P. Jennings, A study on the impact of lithium-ion cell relaxation on electrochemical impedance spectroscopy, J. Power Sources 280 (2015) 74–80.
[50] C. Birkl, D. Howey, Model identification and parameter estimation for LiFePO4 batteries, Hybrid and Electric Vehicles Conference 2013 (HEVC 2013), IET, London, 2013 p. 1–6.
[51] Y. Sheng, Investigation of Electrolyte Wetting in Lithium Ion Batteries: Effect of Electrode Pore Structures and Solution, in Materials Science and Engineering, The University of Wisconsin-Milwaukee: The University of Wisconsin-Milwaukee, 2015 p. 146.
[52] H.-G. Schweiger, O. Obeid, O. Komesker, A. Raschke, M. Schiemann, C. Zehner, M. Gehnen, M. Keller, P. Birke, Comparison of several methods for determining the internal resistance of lithium ion cells, Sensors 2010 (10) (2010) 5604–5625.
[53] D. Zhang, B.S. Haran, A. Durairajan, R.E. White, Y. Podrazhansky, B.N. Popov, Studies on capacity fade of lithium-ion batteries, J. Power Sources 91 (2000) 91–99.
[54] A.B. Stanbridge, A.Z. Khan, D.J. Ewins, Modal testing using impact excitation and a scanning LDV, Shock Vib. 7 (2000) 91–100.
[55] B. Weekes, D. Ewins, Effective use of scanning laser doppler vibrometers for modal tests, Sound Vib. (August) (2016) 8–14.